

# Oxygen Distribution at the Hot Spot in BOF Steelmaking



BERNHARD MITAS and JOHANNES SCHENK

The distribution of oxygen between the gaseous and liquid oxidation products at the hot spot is modeled. The simplified model accurately describes the interaction of the gas jet exiting the lance nozzles with the gaseous surrounding of the jet. This interaction changes the chemical composition of the gas jet influencing the subsequent interaction with the hot spot. The iterative procedure then calculates the chemical composition of the gas exiting the cavity. The characterization of the exiting gas flowing past the lance head as well as the generation rate of FeO is attained by combining the modeled gas composition exiting the cavity with an oxygen mass balance based on a quasi-stationary BOF operation.

<https://doi.org/10.1007/s11663-024-03058-6>  
© The Author(s) 2024

## I. INTRODUCTION

IN BOF steelmaking, gaseous oxygen is blown at supersonic speed onto the liquid hot metal surface, where the gaseous oxygen reacts partially with the entrained gaseous surrounding inside the jet. Decarburization and iron oxidation simultaneously occur at the impingement site of the gas mixture. A requirement for the determination of the gas composition at the impingement site is the gas composition of the surrounding of the gas jet. Even using the given gas composition and velocity field at the impingement site, the determination of the chemical turnover proves to be difficult. The decarburization reaction-limiting mechanisms need to be determined and possible competing reactions considered. For high carbon contents, a literature study suggests that the rate of decarburization would prove limiting by gaseous mass transfer.<sup>[1]</sup>

All models describing emulsion refining depend on assumptions regarding the FeO generation rate. The carbon-refining efficiency estimations of the emulsion are also based on these FeO-generation rates, and various proposed models have used 100 pct oxygen utilization on the hot spot. Chigwedu<sup>[2]</sup> distributed the blown oxygen based on an introduced quantity proportional to the gibbs free energy for the oxidation of the iron-dissolved species and temperature. Lytvynyuk<sup>[3]</sup> and Bundschuh<sup>[4]</sup>

modeled the mass transfer over the metal–emulsion interface and the reactions occurring inside the emulsion. Since there was no separate hot spot model, all of the impinging oxygen were transformed to FeO. Similarly, Sarkar<sup>[5]</sup> distributed oxygen based on the weight fraction of the species available at the hot spot (Reactor 2). Dogan<sup>[6]</sup> used Sherwood number correlations presented for the impinging gas jets onto a liquid to calculate the mass transfer of oxygen and carbon dioxide through the gaseous boundary layer. A fixed off gas recirculation rate of 10 pct was used to calculate the gas composition at the hot spot. The hot spot off gas composition was assumed to be invariant (85 pct CO and 15 pct CO<sub>2</sub>).<sup>[7]</sup> It was also assumed that the bottom plug purging gases would be present at the hot spot and the FeO generation was not modeled. Based on the measured chemical compositions by Cicutti,<sup>[8]</sup> a predefined chemical pathway for the slag composition was chosen. The presented calculations started using an assumed initial decarburization value of 120 kg [C]/min.<sup>[9]</sup> This carbon was divided using the mentioned fixed ratio of CO/CO<sub>2</sub> leading in turn to a new decarburization rate. The hot spot model by Dogan<sup>[6]</sup> is in essence a iterative model which was iterated jointly with the blowing time thus explaining the oscillation phenomena in Figure 1. When the initial decarburization rate is higher than the solution of the iterative procedure, a higher fraction of CO<sub>2</sub> and a lower fraction of O<sub>2</sub> are present at the reaction site. Since oxygen is the stronger decarburization agent, the lowering of oxygen partial pressure leads to a lower total decarburization rate, which in turn leads to an elevated oxygen partial pressure. With blowing time progression, the partial pressure in Figure 1 approaches the solution for the defined blowing conditions. When the blowing conditions change, the next solution is approached with progressing calculation steps and therefore blowing time.

BERNHARD MITAS and JOHANNES SCHENK are with the Chair of Ferrous Metallurgy, Montanuniversitaet Leoben, 8700 Leoben, Austria and also with the K1-MET GmbH, 4020 Linz, Austria. Contact e-mail: [bernhard.mitas@stud.unileoben.ac.at](mailto:bernhard.mitas@stud.unileoben.ac.at)

Manuscript submitted June 21, 2023; accepted February 24, 2024.

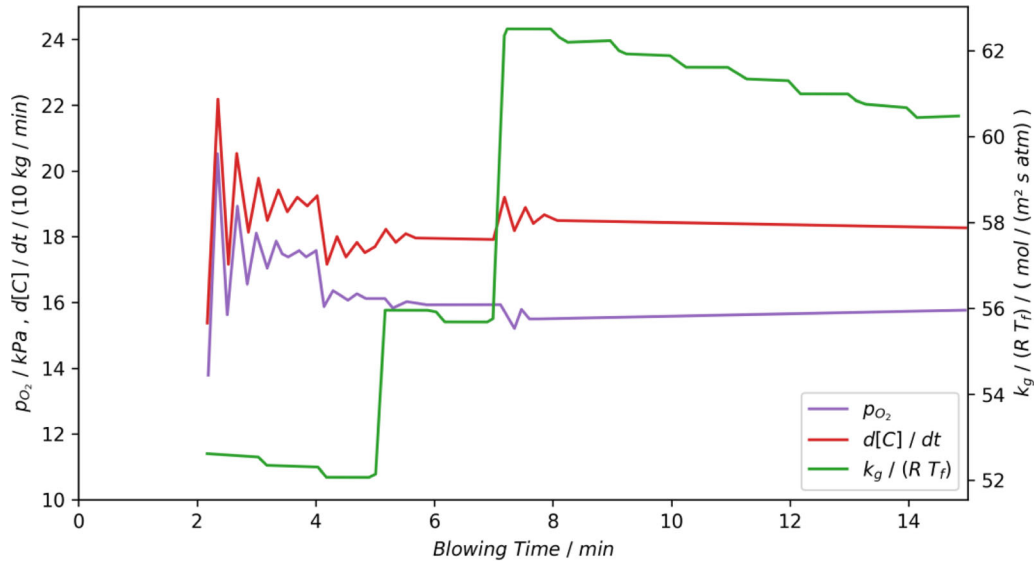


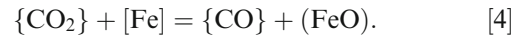
Fig. 1—Behavior of decarburization rate, oxygen partial pressure, and mass transfer coefficient during a blow according to results taken from Dogan.<sup>[6]</sup>

The presented model's aspiration is to analytically describe the oxygen distribution as simple as possible providing illustrative clarity. It is necessary to mention that although the hot spot phenomena involve a multi-phase flow problem (gas impinging onto a liquid), it is not necessary to address the modeling of the hot metal boundary layer for the main duration of the blow. This is due to the limitation of the mass transfer being attributed to the mass transfer through the gaseous boundary layer for carbon contents of the hot metal greater than the critical carbon content. Thus, this model is valid for carbon contents of the hot metal above approximately 0.07 to 0.3 wt pct<sup>[10]</sup> and can be easily extended to achieve validity for the full blowing duration.

## II. MODEL INTRODUCTION

The model depicts a system of well-understood physical sub-models and phenomena. The free turbulent jet and the flow along a flat plate are main components of the model system. The findings are calculated for a single oxygen jet, therefore the influence of multiple oxygen jets on each other is not included. The entrainment behavior of the oxygen jet in the converter is modeled as comparable to a free turbulent jet. It is also assumed that the mixing and reaction kinetics are sufficiently fast/swift at all lance heights, in other words, ensuring that all gases entrained with the potential to react, will do so. The gas jet, containing the reaction products, interacts with the hot spot. The reaction-limiting step is taken as the mass transfer through the gaseous boundary layer. This assumption is considered to be sufficiently accurate for high iron oxidation rates, where the liquid boundary layer is consumed due to the reaction. The assumption can be valid, due to intensive

interaction of the impinging jet and therefore enhancing the mixing of the hot metal. The reaction-controlled mechanism was disregarded as it was found that hot spot temperatures can exceed well over 2000 °C<sup>[11]</sup> and even at lower temperatures, these phenomena play a subservient role.<sup>[1]</sup> The total species transport to the hot spot is proportional to the area of the cavity (calculated using the model of Koria<sup>[12]</sup>), and the specific species transport through the gaseous boundary layer (using Eq. [5]). The gaseous reactants considered regarding the reactions occurring at the hot spot are oxygen and carbon dioxide. The considered reactions are shown in Eqs. [1] through [4].



Oeters<sup>[13]</sup> investigated the kinetics of the decarburization reaction using carbon dioxide, which is shown in Eq. [3]. The reaction products are forced to flow against the oncoming reaction educts, therefore inhibiting the reaction speed. The reaction systems classification based on the number of gaseous molecules created per gaseous molecule of oxygen or carbon dioxide is shown in Table I, where  $\chi^\infty$  is the molar fraction of the gaseous reactant in outside the boundary layer and  $\chi^*$  is the equilibrium molar fraction of the species on the interface.

The entrainment of the surrounding is shown on the right-hand side of Figure 2. On the left-hand side there is a loop indicating that the volume flow of the jet can exceed the volume flow of oxygen. Subsequent to the entrainment of the surrounding, the generated gas mixture is combusted in an infinitesimal small combustion volume close to the hot spot. The combusted gases, including superfluous carbon monoxide, interact at the hot spot. The amount of reactant transferred to the hot spot is calculated using the gas flows stagnation pressure and the axial velocity at the hot spots position. The reaction products of the hot spot form the new surrounding, which in turn is entrained. Using this iterative approach, the surrounding composition can then be calculated.

Equation [5] is used to calculate the Sherwood number regarding the mass transfer through the gas boundary layer at the hot spot. It is valid for Reynolds numbers greater than  $2 \times 10^5$ .<sup>[14]</sup> All calculations performed fulfilled the Reynolds criteria for turbulent flow. The effect of the local turbulences past the laminar layer on the mass transfer coefficient is considered when using the given Sherwood number equation. In this model, the gaseous boundary layer determines the mass transfer and therefore the modeling of the liquid phase proves superfluous. For low carbon contents of the hot metal ( $< 0.07$  to  $0.3$  wt pct<sup>[10]</sup>), it would be required and advised to calculate the influence of the carbon transport through the liquid boundary layer.

$$Sh_L = 0.0365Re^{4/5}Sc^{1/3}. \quad [5]$$

**Table I. Kinetic Proportionality Factors for Considered Reactions**

Equation Name	Number of Gaseous Reaction Products	Proportionality Factor for Reaction Kinetics
$G_{O_2+2C=2CO}$	2	$\ln\left(\frac{1+\chi^\infty}{1+\chi^*}\right)^{[13]}$
$G_{O_2+2Fe=2FeO}$	0	$\ln\left(\frac{1-\chi^*}{1-\chi^\infty}\right)$
$G_{CO_2+C=2CO}$	2	$\ln\left(\frac{1+\chi^\infty}{1+\chi^*}\right)^{[13]}$
$G_{CO_2+Fe=CO+FeO}$	1	$\chi^\infty - \chi^*$

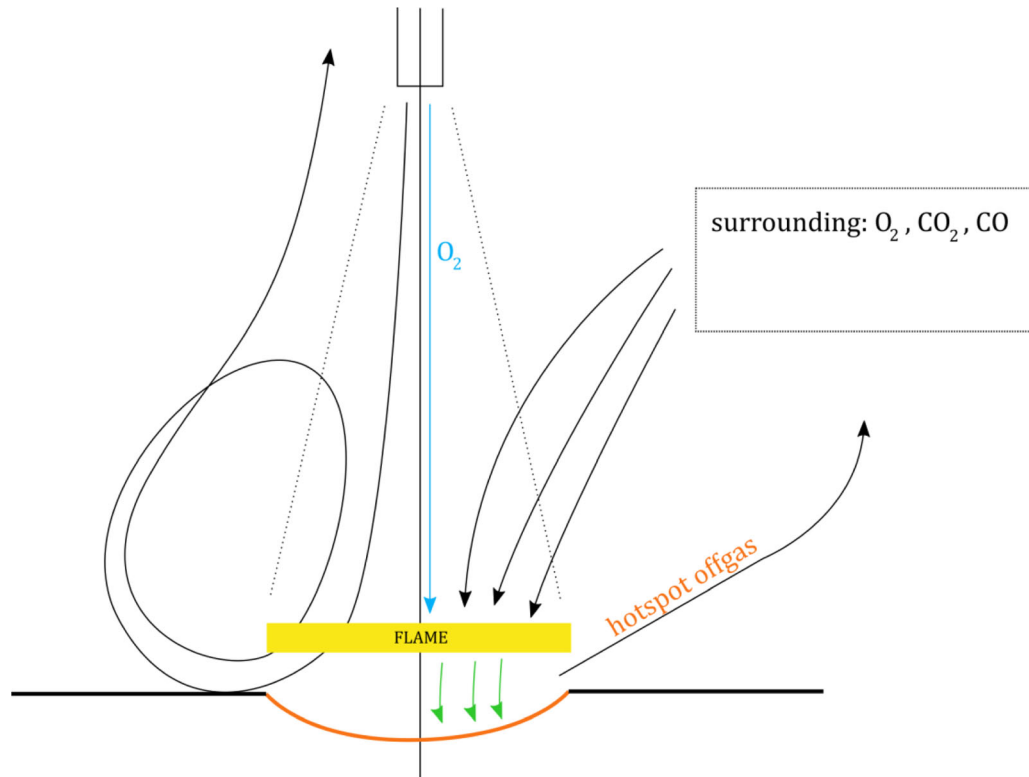


Fig. 2—Model concept: flame and hot spot reaction zones and schematic stream lines.

### III. MODEL DESCRIPTION

The partial normal volume flows of species are written in vector form for brevity, see Eq. [6]. When applying the presented iterative approach to a set of blowing conditions, the functions in Eqs. [7] to [9] are solved. As depicted below, the function *hotspot* calculates the composition changes of the gas due to the reactions there. The function *flame* calculates the oxidation of the entrained gases taken from the surrounding of the jet. The function *mixing* calculates the gas composition after the reactionless entrainment of the surrounding. These functions are interconnected by Eqs. [10] to [12]. The iterative formula in Eq. [13] is solved using a pure carbon monoxide surrounding as the starting point.

$$\underline{\dot{V}} = \begin{pmatrix} \dot{V}_{O_2} \\ \dot{V}_{CO_2} \\ \dot{V}_{CO} \end{pmatrix} \quad [6]$$

$$\underline{\dot{V}}_{hotspot}^{out} = hotspot(\underline{\dot{V}}_{hotspot}^{in}) \quad [7]$$

$$\underline{\dot{V}}_{flame}^{out} = flame(\underline{\dot{V}}_{flame}^{in}) \quad [8]$$

$$\underline{\dot{V}}_{mixing}^{out} = mixing(\underline{\dot{V}}_{mixing}^{in}) \quad [9]$$

$$\underline{\dot{V}}_{hotspot}^{in} = \underline{\dot{V}}_{flame}^{out} \quad [10]$$

$$\underline{\dot{V}}_{flame}^{in} = \underline{\dot{V}}_{mixing}^{out} \quad [11]$$

$$\underline{\dot{V}}_{mixing}^{in} = \underline{\dot{V}}_{hotspot}^{out} \quad [12]$$

$$\underline{\dot{V}}_{hotspot}^{out^{(n+1)}} = hotspot(flame(mixing(\underline{\dot{V}}_{hotspot}^{out^{(n)}}))). \quad [13]$$

The *mixing* function calculates the gas composition of the jet prior to the combustion of the entrained volume elements using Eqs. [14] and [15]. The normal volume flow of the surrounding into the gas jet  $\dot{V}_h$  is calculated using the total volume flow of the gas jet at the distance  $h$  from the nozzle (based on the free turbulent jet). The subtraction of the normal volume flow of oxygen blown from the total flow results in the entrained flow  $\dot{V}_h$ .

Initially, the molar ratios of the entrained gases  $\underline{\dot{V}}_{mixing}^{in}$  are calculated. The normal volume flow of the mixed jet prior to the homogeneous gas combustion  $\underline{\dot{V}}_{mixing}^{out}$  is calculated by adding the oxygen flow rate of the blowing lance  $\dot{V}_{O_2BL}$  to the entrained gas stream.

$$\underline{\dot{V}}_{mixing}^{in} = \frac{\underline{\dot{V}}_{mixing}^{in}}{\text{sum}\{\underline{\dot{V}}_{mixing}^{in}\}} \quad [14]$$

$$\underline{\dot{V}}_{mixing}^{out} = \begin{pmatrix} \dot{V}_{O_2BL} \\ 0 \\ 0 \end{pmatrix} + \underline{\dot{V}}_{mixing}^{in} \dot{V}_h K_T. \quad [15]$$

The *flame* function calculates the homogeneous gaseous reaction inside the gas jet as Eqs. [16] to [20] indicate. Equation [17] limits the combustible quantity of carbon monoxide by the available amount inside the gas stream.

$$\underline{\dot{V}}_{flame}^{in} = \begin{pmatrix} \dot{V}_{O_2}^{in} \\ \dot{V}_{CO_2}^{in} \\ \dot{V}_{CO}^{in} \end{pmatrix} \quad [16]$$

$$\dot{V}_{CO}^{out} = \begin{cases} \dot{V}_{CO}^{in} - 2\dot{V}_{O_2}^{in}, & 0 < \dot{V}_{O_2}^{in} < \frac{1}{2}\dot{V}_{CO}^{in} \\ 0, & \dot{V}_{O_2}^{in} \geq \frac{1}{2}\dot{V}_{CO}^{in} \end{cases} \quad [17]$$

$$\dot{V}_{CO_2}^{out} = \dot{V}_{CO_2}^{in} - (\dot{V}_{CO}^{out} - \dot{V}_{CO}^{in}) \quad [18]$$

$$\dot{V}_{O_2}^{out} = \dot{V}_{O_2}^{in} + \frac{1}{2}(\dot{V}_{CO}^{out} - \dot{V}_{CO}^{in}) \quad [19]$$

$$\underline{\dot{V}}_{flame}^{out} = \begin{pmatrix} \dot{V}_{O_2}^{out} \\ \dot{V}_{CO_2}^{out} \\ \dot{V}_{CO}^{out} \end{pmatrix}. \quad [20]$$

The *hotspot* function calculates compositional changes of the gas stream due to hot spot reactions *via* Eqs. [21] to [38]. The normal volume flow of the hot spot active gases is calculated using Eq. [22]. Carbon monoxide does not appear as reactant in the considered chemical reactions seen in Eqs. [1] to [4].

$$\underline{\dot{V}}_{hotspot}^{in} = \begin{pmatrix} \dot{V}_{O_2}^{in} \\ \dot{V}_{CO_2}^{in} \\ \dot{V}_{CO}^{in} \end{pmatrix} \quad [21]$$

$$\dot{V}_{ha}^{in} = \dot{V}_{O_2}^{in} + \dot{V}_{CO_2}^{in} \quad [22]$$

$$\underline{\chi} = \frac{\dot{V}_{hotspot}^{in}}{\text{sum} \left\{ \dot{V}_{hotspot}^{in} \right\}}. \quad [23]$$

The normal volume flow of reactants consumed due to the hot spot reactions is calculated by applying Eqs. [5] to [24] and [25], where  $u$  is the gas velocity along the cavity outside the boundary layer,  $L$  is the length of the curve from the center to the end (modeled as circular paraboloid),  $\rho$  is the gas density inside the cavity,  $D$  is the mass diffusivity, and  $\eta$  is the dynamic viscosity of the gas.

$$\text{Re} = \frac{uL\rho}{\eta} \quad [24]$$

$$\text{Sc} = \frac{\eta}{\rho D} \quad [25]$$

The specific mass flow  $\frac{\dot{m}}{A}$  of the gaseous educts towards the interface is calculated *via* Eq. [26], where  $\chi_\infty$  is the volume fraction of the reactive gases outside the boundary layer and  $\chi_i$  is the volume fraction of the reactive gases at the interface which is taken as zero. Using Eq. [27], the normal volume flow of reactive gases through the boundary layer is calculated taking into account the density of the gases at normal conditions  $\rho_N$ , the area of the hot spot  $A$ , and the model factor  $K_\beta$ .

$$\frac{\dot{m}}{A} = \frac{\text{Sh}_L D}{L} \rho (\chi_\infty - \chi_i) \quad [26]$$

$$\dot{V}_\beta = \frac{\dot{m}}{A} \frac{1}{\rho_N} A K_\beta \quad [27]$$

The ratio  $\Psi$  of the hot spot reaction volume flow  $\dot{V}_\beta$  and the volume flow of possible reactant species  $\dot{V}_{ha}^{in}$  is calculated using Eq. [28].

$$\Psi = \begin{cases} \frac{\dot{V}_\beta}{\dot{V}_{ha}^{in}}, & 0 < \frac{\dot{V}_\beta}{\dot{V}_{ha}^{in}} < 1 \\ 1, & \frac{\dot{V}_\beta}{\dot{V}_{ha}^{in}} \geq 1 \end{cases} \quad [28]$$

It is assumed that every molecule of reactant is immediately consumed when reaching the interface. Since the reactants of considered chemical reactions do not appear on the product side, the amount of carbon dioxide and oxygen in the cavity off gas can be calculated using Eqs. [29] and [30].

$$\dot{V}_{O_2}^{out} = (1 - \Psi) \dot{V}_{O_2}^{in} \quad [29]$$

$$\dot{V}_{CO_2}^{out} = (1 - \Psi) \dot{V}_{CO_2}^{in} \quad [30]$$

The normal volume flow of carbon monoxide produced *via* carbon dioxide as oxygen carrier  $\dot{V}_{CO}^{CO_2}$  is calculated using Eq. [31]. The normal volume flow of carbon dioxide reacting at the hot spot is equal to the product of  $\Psi \dot{V}_{CO_2}^{in}$ . This product is weighted using the factors presented in Table I. Using Eq. [34], the normal volume flow of carbon monoxide exiting the hot spot reactor is calculated using partial normal volume flows from Eqs. [31] to [33].

$$\dot{V}_{CO}^{CO_2} = \Psi \dot{V}_{CO_2}^{in} \frac{G_{CO_2+C=2CO}}{G_{CO_2+C=2CO} + G_{CO_2+Fe=CO+FeO}} \quad [31]$$

$$\dot{V}_{CO}^{O_2} = 2\Psi \dot{V}_{O_2}^{in} \frac{G_{O_2+2C=2CO}}{G_{O_2+2C=2CO} + G_{O_2+2Fe=2FeO}} \quad [32]$$

$$\dot{V}_{CO}^{FeO} = \Psi \dot{V}_{CO_2}^{in} \frac{G_{CO_2+Fe=CO+FeO}}{G_{CO_2+C=2CO} + G_{CO_2+Fe=CO+FeO}} \quad [33]$$

$$\dot{V}_{CO}^{out} = \dot{V}_{CO}^{in} + \dot{V}_{CO}^{CO_2} + \dot{V}_{CO}^{O_2} + \dot{V}_{CO}^{FeO}. \quad [34]$$

Similarly, the same procedure is applied to the iron oxide generation using Eqs. [35] to [37]. The volume flow of iron oxide is taken as ideal gas at normal conditions for calculation and comparison purposes.

$$\dot{V}_{FeO}^{O_2} = 2\Psi \dot{V}_{O_2}^{in} \frac{G_{O_2+2Fe=2FeO}}{G_{O_2+2C=2CO} + G_{O_2+2Fe=2FeO}} \quad [35]$$

$$\dot{V}_{FeO}^{CO_2} = \Psi \dot{V}_{CO_2}^{in} \frac{G_{CO_2+Fe=FeO+CO}}{G_{CO_2+C=2CO} + G_{CO_2+Fe=CO+FeO}} \quad [36]$$

$$\dot{V}_{FeO}^{out} = \dot{V}_{FeO}^{O_2} + \dot{V}_{FeO}^{CO_2} \quad [37]$$

$$\underline{\dot{V}}_{hotspot}^{out} = \begin{pmatrix} \dot{V}_{O_2}^{out} \\ \dot{V}_{CO_2}^{out} \\ \dot{V}_{CO}^{out} \end{pmatrix}. \quad [38]$$



When calculating the mass transfer through the gaseous boundary layer (see calculation of  $\dot{V}_\beta$ ), the type of reaction and the amount of produced mole gas per mole reactant influencing the mass flow through the boundary layer are omitted. On the other hand, when calculating the distribution of a specific reactant ( $\text{CO}_2$  or  $\text{O}_2$ ) between the competing reactions, these mechanisms are taken into account.

#### IV. THE MODEL RESULTS

The presented model is applied to a hypothetical industrial size converter using the parameters exhibited in Table II. Two factors for modifying the calculation are introduced. The mass transfer through the boundary layer is multiplied with the factor  $K_\beta$  and the volume flow entrained into the gas jet is multiplied with the factor  $K_T$ .

The dimensionless entrainment constant  $K_T$  was chosen as the number one half. The jets exiting industrial multi-hole lances experience off gas surrounding only at the perimeter of the jet battery. As a first approximation, it is assumed that half of a single jet is contacting the off gas surrounding and the other half the remaining oxygen jets. Further calculations are performed using a 1/10 of the mentioned value in order to examine the influence of the entrainment constant on the attained results. The value of  $K_T = 0.05$  is therefore the chosen arbitrary used to demonstrate the variation of the model constant on the model results. The chosen hot spot gas consumption factors  $K_\beta$  coincide with the observed values for flame collapse at certain lance heights when combined with the previously mentioned entrainment factors ( $K_\beta = 40$  for  $K_T = 0.5$  and  $K_\beta = 20$  for  $K_T = 0.05$ ).<sup>[15]</sup> The values of  $K_\beta$  are found by adjusting the carbon monoxide concentration of the off gas to the lower carbon monoxide explosion limit at the lance height, where flame collapse can be observed in industrial converters.

As depicted in Figure 3, the iron oxidation is favored at low lance heights, because there is less entrainment of the surrounding and the oxygen content of the impinging jet is higher. The iron oxidation is kinetically favored for the reactant molecular oxygen as seen in Table I and oxygen is distributed to the iron oxidation reaction rather than carbon oxidation reaction at low lance heights. The comparison of Figures 3(a) with (b) reveals that higher entrainment rates of the surrounding,

achieved through higher entrainment factors  $K_T$ , lead to a steeper fall of the iron oxidation rate. The comparison of Figures 3(a) and (c) indicates that an increasing hot spot gas consumption factor moves the first break point to higher lance heights. From this the break point on, to higher lance heights, the mass transfer to the gaseous boundary layer at the hot spot proves insufficient. A quantity of potentially reactive gaseous species cannot react anymore.

Figure 4 depicts the partial normal volume flow of species exiting the modeled system indicated by continuous lines. The dotted lines represent the partial normal volume flows after utilization of available oxygen for carbon monoxide combustion. The dotted lines thus represent post-combustion (pc) values meaning "post-modeled-system-combustion." The comparison of Figures 3 and 4 unveils the second break point marking the onset of unused oxygen leaving the modeled system. The former mentioned unused oxygen is "post combusted" with available carbon monoxide soon after the lance head. One part of the blown oxygen reacts to FeO, which is subsequently a potential reactant for the decarburization inside the emulsion phase (not included in this model). The volume flow quantities in the presented figure related to the post-combusted state as well as the sum of gaseous species are shown in volume flow per gas species. The values before the post-combustion are molecular oxygen.

Figure 5 depicts the fraction of hot spot decarburization for 4 m lance height to 90 pct and for 6 m lance height to 95 pct, when taking  $K_\beta = 40$  and  $K_T = 0.5$ . For these two lance heights, as Figure 4(d) indicates, the oxygen utilization is 100 pct. Even for a lance height of 6 m, oxygen is absent in the exiting gas of the hot spot reactor.

Although various researches predicted lower hot spot decarburization fractions, the quantity is still in discussion. Dogan<sup>[7]</sup> predicted hot spot decarburization fractions of 55 pct for the calculation conditions of Cicutti.<sup>[8]</sup> For this 200t converter analyzed by Cicutti,<sup>[8]</sup> the lance heights were between 2.5 and 1.8 m. The model results presented in this work would be applicable to predict conditions found in converter with specifications as seen in Table II. The hot spot decarburization fractions were found to be approximately 80 pct for lance heights between 2.5 and 1.8 m. Chatterjee<sup>[16]</sup> estimated that 40 to 50 pct of decarburization occurs in the impact zone and the slag-metal interface and the remaining 60 to 50 pct would occur in the emulsion. These findings were based on experimental investigations using 0.5 m lance height and a 64 mm and 16 mm nozzle. The present model, with a nozzle diameter between the two used nozzles by Chatterjee,<sup>[16]</sup> predicts decarburization fractions in the same range around 50 pct for 0.5 m lance height.

It was argued that, when considering significant fractions of emulsion decarburization, a physical limit for the foam volume needs to be considered. When a certain volume stream of decarburization products is generated on random positions in a liquid slag phase, the foam expansion can be estimated using foam index

Table II. Calculation Conditions

Description	Quantity
Stagnation Pressure	10 bar
Norm Volume Flow Nozzle	10 Nm <sup>3</sup> /s
Critical Diameter Nozzle	30 mm
Equilibrium Oxygen Partial Pressure	1E-6 bar
Dynamic Viscosity	19 μ Pa s
Diffusion Coefficient	17 μ m s <sup>-1</sup>

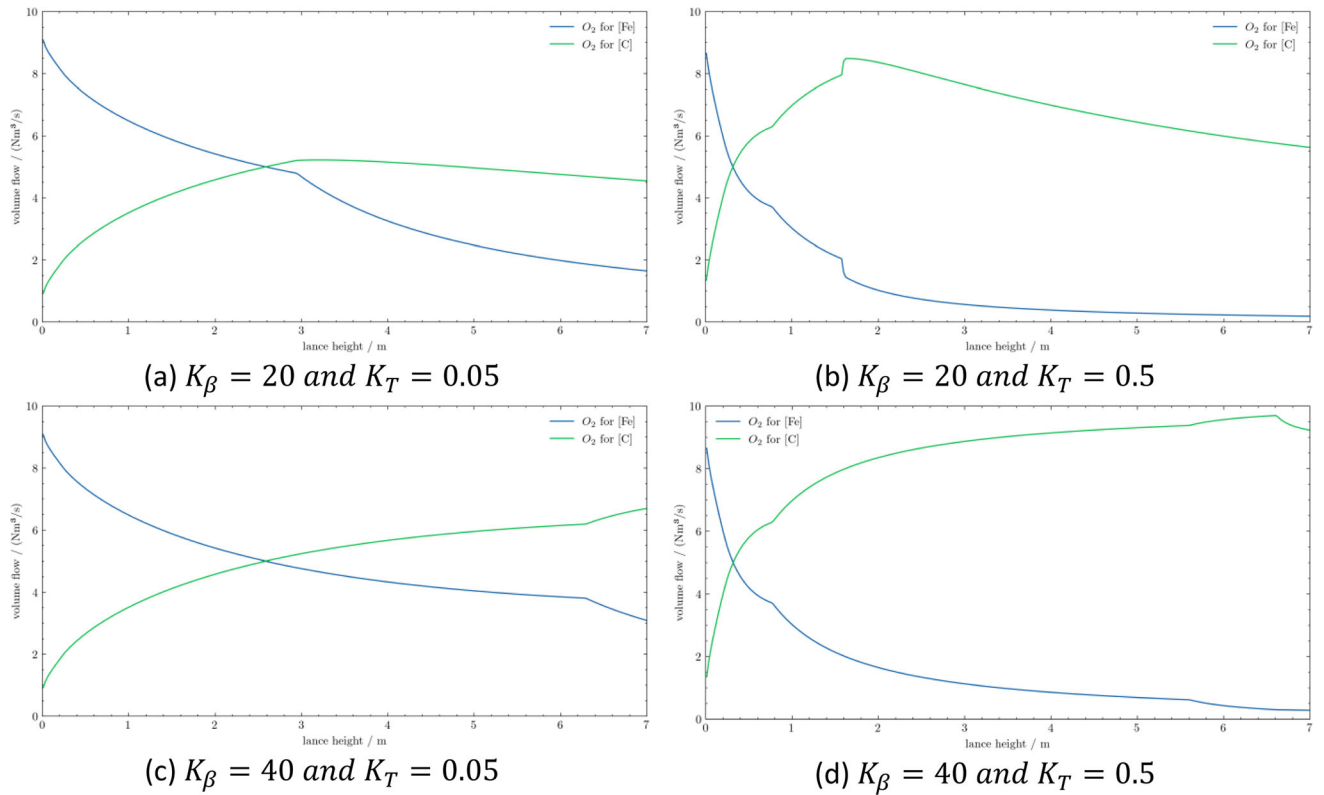


Fig. 3—Oxygen distribution regarding the decarburization and iron slagging for (a)  $K_\beta = 20$  and  $K_T = 0.05$ , (b)  $K_\beta = 20$  and  $K_T = 0.5$ , (c)  $K_\beta = 40$  and  $K_T = 0.05$ , and (d)  $K_\beta = 40$  and  $K_T = 0.5$ .

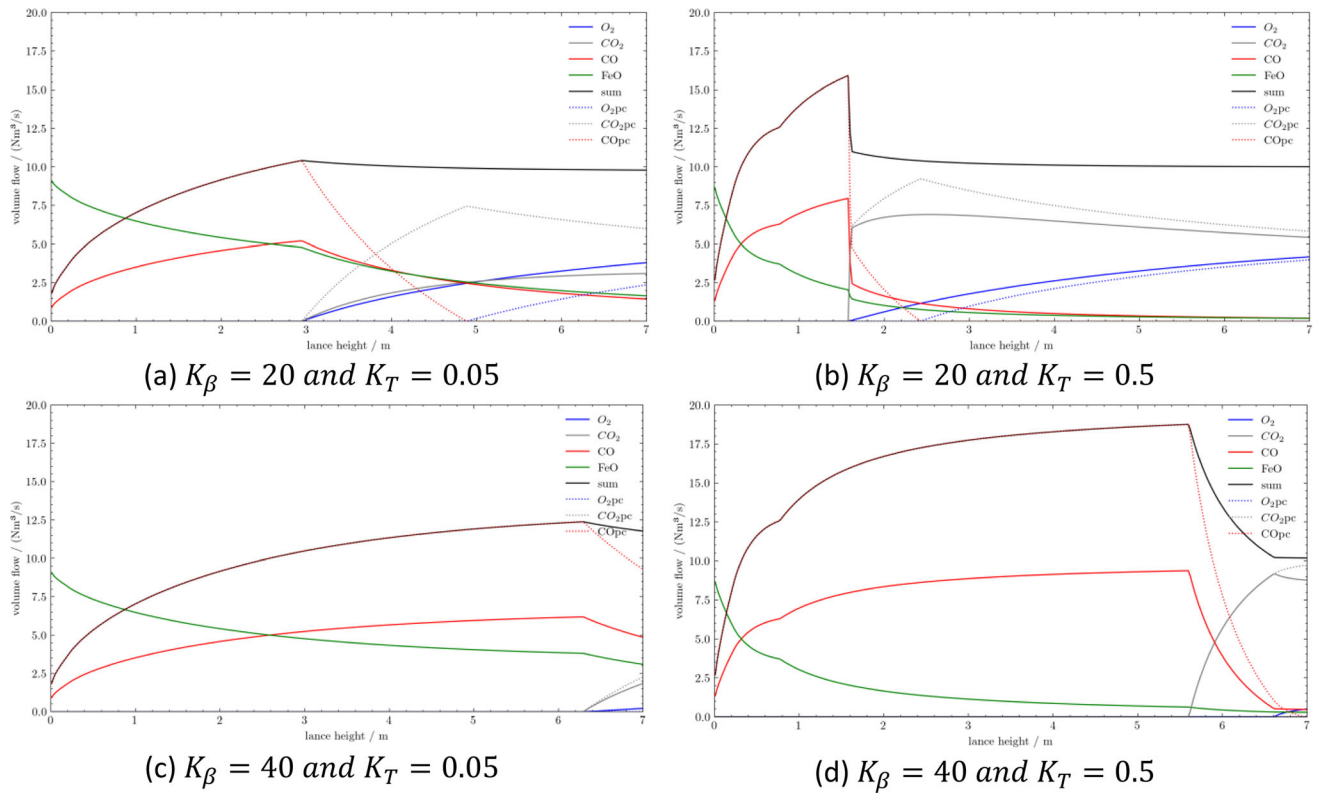


Fig. 4—Gas composition exiting the hot spot (solid lines) and passing the lance head (exiting the modeled system) (broken lines) for (a)  $K_\beta = 20$  and  $K_T = 0.05$ , (b)  $K_\beta = 20$  and  $K_T = 0.5$ , (c)  $K_\beta = 40$  and  $K_T = 0.05$ , and (d)  $K_\beta = 40$  and  $K_T = 0.5$ .

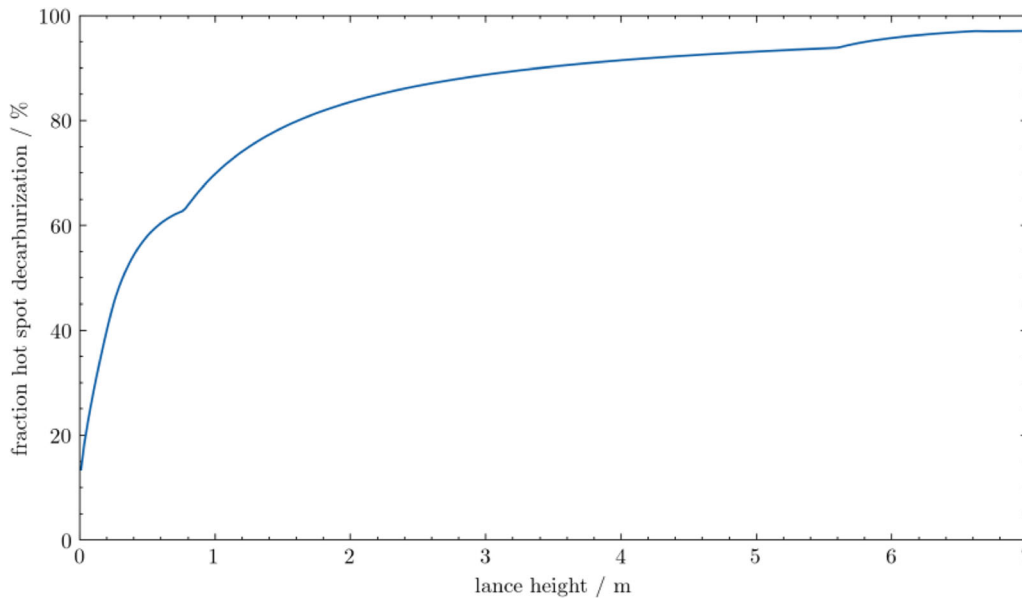


Fig. 5—Fraction of hot spot decarburization on total decarburization for various lance heights and  $K_{\beta} = 40$  and  $K_T = 0.5$ .

models. It was estimated that the emulsion decarburization should be < 25 pct that a 200t converter vessel operates without slopping.<sup>[17]</sup>

## V. CONCLUSION

The aim of this research is to create a simplified but universal model which is still able to predict the oxidation of elements in the hot metal phase accurately. The multi-phase flow of the modeled vessel section is considered, however, the mass transfer through the liquid hot metal is sufficiently enhanced so that the overall mass transfer is only limited by the gaseous boundary layer. In order to create this model, the multi-phase flow problem is considered to be reduced to a single-phase flow problem. In this research and its resulting iterative model, the gas composition subsequent to the hot spot reaction and the FeO generation rate is determined and illustrated. It then depicts the fraction of decarburization occurring at the hot spot and investigates the post-combustion ratios dependence on the lance height. The model uses the entrainment of a single oxygen jet entering a quiescent homogenous surrounding as the entrainment of an oxygen jet exiting from a multi-hole lance into the BOF vessel. The species transfer at the hot spot is taken to be limited by the transfer through the gas boundary layer and calculated using Sherwood equations presented for the flat plate. The reactants for the hot spot reactions, oxygen and carbon dioxide, are distributed based on kinetic factors calculated using one-dimensional forced diffusion equations. Using a forty times higher mass transfer rate results in consonance of predicted and observed flame collapse lance heights. Hot spot decarburization fractions at low lance heights (0.5 m) agree well with

measurements by Chatterjee.<sup>[16]</sup> For lance heights between 2.5 and 1.8 m, the model predicts hot spot decarburizations fraction of 80 pct compared with previously predicted values of 55 pct.<sup>[7]</sup> The gas transfer through the boundary layer is calculated independently from the occurring reactions. The iron oxidation reaction results in a gas sink on the gas-liquid interface leading to higher net gas transfer rates through the boundary layer, possibly explaining the observed deviations.

The first principle model yields process quantities which were previously inaccessible by available models like the post-combustion ratio, the oxygen distribution between hot spot and emulsion reaction systems, and the lance height-dependent oxygen utilization. The model serves as a basis for emulsion-refining models and post-combustion calculations. The insight into lance height dependences of process quantities is of significance since the variation of lance height is one of the most crucial tools for process adjustment. The amount of oxygen used for iron oxidation could be distributed to various non-gaseous oxidation products, for example via the technique developed by Chigwedu.<sup>[2]</sup> In future research models, it would be of significant interest to extend the findings of this model to include the influence of multi-hole lances and temperature effects on the occurring reactions.

To model the oxygen distribution and post-combustion during the BOF Process, the following itemization of the converter is recommended:

- The inverse flame combustion zone where entrained surrounding is combusted using gaseous oxygen
- The hot spot where the impinging gas mixture reacts with in liquid iron-dissolved components and liquid iron itself



- The combustion shortly past the lance head where unused oxygen is combusted with generated carbon monoxide
- The emulsion where at the hot spot generated FeO reacts with carbon-containing droplets producing carbon monoxide
- The post-slag combustion where the off gas stream from shortly past the lance head mixes with the off gas from the emulsion
- The post-converter combustion where the converter off gas mixes with air from outside the converter

### ACKNOWLEDGMENTS

The authors appreciatively acknowledge the funding support of K1-MET GmbH, metallurgical competence center. The research program of the K1-MET competence center is supported by COMET (Competence Center for Excellent Technologies), the Austrian program for competence centers. COMET is funded by the Federal Ministry for Climate Action, Environment, Energy, Mobility, Innovation and Technology, the Federal Ministry for Labour and Economy, the Federal States of Upper Austria, Tyrol, and Styria as well as the Styrian Business Promotion Agency (SFG) and the Standortagentur Tyrol. Furthermore, Upper Austrian Research continuously supports K1-MET. Besides the public funding from COMET, the current research work of K1-MET is partially financed by the participating scientific partner Montanuniversität Leoben and the industrial partners Primetals Technologies Austria GmbH, RHI Magnesita GmbH, and voestalpine Stahl GmbH.

### CONFLICT OF INTEREST

The corresponding author states that there is no conflict of interest.

### FUNDING

Open access funding provided by Montanuniversität Leoben.

### OPEN ACCESS

This article is licensed under a Creative Commons Attribution 4.0 International License, which permits use, sharing, adaptation, distribution and reproduction in any medium or format, as long as you give appropriate credit to the original author(s) and the source, provide a link to the Creative Commons licence, and indicate if changes were made. The images or other third party material in this article are included in the article's Creative Commons licence, unless indicated otherwise in a credit line to the material. If

material is not included in the article's Creative Commons licence and your intended use is not permitted by statutory regulation or exceeds the permitted use, you will need to obtain permission directly from the copyright holder. To view a copy of this licence, visit <http://creativecommons.org/licenses/by/4.0/>.

### NOMENCLATURE

$A$	Area ( $m^2$ )
$D$	Mass diffusivity ( $m^2/s$ )
$G$	Kinetic model factor (1)
$K_\beta$	Model factor regarding mass transfer (1)
$K_T$	Model factor regarding jet entrainment (1)
$L$	Length (m)
$\dot{m}$	Mass flow rate (kg/s)
$u$	Velocity (m/s)
$\dot{V}$	Normal volume flow ( $Nm^3/s$ )

### GREEK LETTER

$\eta$	Dyn. viscosity (Pa s)
$\rho$	Density ( $kg/m^3$ )
$\chi$	Molar fraction (1)
$\Psi$	Reaction ratio (1)

### SUBSCRIPT

$h$	Quantity at lance height (near hot spot)
$ha$	Hot spot active
$N$	Quantity at normal conditions (20 °C, 1atm)

### SUPERSCRIPT

$\infty$	Quantity outside the boundary layer
*	Quantity at the interface

### BRACKETS

[Element of periodic table]	Mass fraction of element dissolved in liquid iron
(Element of periodic table)	Mass fraction of element dissolved in slag
{Element of periodic table}	Mass fraction of element in gas phase

## REFERENCES

1. Y. Fan, X. Hu, H. Matsuura, and K. Chou: *ISIJ Int.*, 2023, vol. 63, pp. 10–19.
2. C. Chigwedu, J. Kempken, and W. Pluschkell: *Stahl Eisen*, 2006, vol. 126, pp. 25–31.
3. Y. Lytvynuk, J. Schenk, M. Hiebler, and H. Mizelli: *6th EOSC European Oxygen Steelmaking Conference*, 2011.
4. P. Bundschuh: *Thermodynamische und kinetische Modellierung von LD-Konvertern*. Dissertation, Leoben, 2017.
5. R. Sarkar, P. Gupta, S. Basu, and N.B. Ballal: *Metall. Trans. B*, 2015, vol. 46B, pp. 961–76.
6. N. Dogan, G.A. Brooks, and M.A. Rhamdhani: *ISIJ Int.*, 2011, vol. 51, pp. 1102–09.
7. N. Dogan, G.A. Brooks, and M.A. Rhamdhani: *ISIJ Int.*, 2011, vol. 51, pp. 1086–92.
8. C. Cicutti, M. Valdez, T. Pérez, J. Petroni, A. Gomez, R. Donayo, and L. Ferro: *6th International Conference on Molten Slags, Fluxes and Salts*, 2000.
9. N. Dogan: *Mathematical Modelling of Oxygen Steelmaking*. PhD Thesis, Melbourne, Australia, 2011.
10. A.K. Shukla, B. Deo, S. Millman, B. Snoeijer, A. Overbosch, and A. Kapilashrami: *Steel Res. Int.*, 2010, vol. 81, pp. 940–48.
11. K. Koch, W. Fix, and P. Valentin: *Arch. Eisenhüttenwes.*, 1978, vol. 49, pp. 163–66.
12. S.C. Koria and K.W. Lange: *Steel Res.*, 1987, vol. 58, pp. 421–26.
13. F. Oeters: *Metallurgie der Stahlherstellung*, Springer, Berlin, 1989.
14. J.R. Welty, G.L. Rorrer, and D.G. Foster: *Fundamentals of momentum, heat, and mass transfer*, 7th ed. Wiley, Hoboken, 2019.
15. W. Resch: *Die Kinetik der Entphosphorung beim Sauerstoffaufblasverfahren für phosphorreiches Roheisen*. Dissertation, 1976.
16. A. Chatterjee, N. Lindfors, and J. Weste: *Ironmaking Steelmaking*, 1976, vol. 1, pp. 21–32.
17. B. Mitas, V.-V. Visuri, and J. Schenk: *Metall. Trans. B*, 2023, vol. 54B, pp. 1938–53.

**Publisher's Note** Springer Nature remains neutral with regard to jurisdictional claims in published maps and institutional affiliations.